

Dear Dr Ben Mirus,

Thank you for your nice and constructive comments. We have addressed your comments point-by-point and provided the answer, explanation, and modification where are required in the revised manuscript. This has been uploaded as a supplement file where you can find our answers in a table plus the revised manuscript with track changes.

We hope our answers satisfy your demands.

Best regards,

Jalal Samia and the co-authors

Referee's comments:

Authors responses :

Comment	Response
<p>General Comment:</p> <p>Given the superior performance of the “path dependent only” model over the “conventional” model, it is important to note that at least the spatial part of the path dependent model may not be entirely related to the occurrence of past landslides. Rather this might also be at least partially explained by the generally accepted phenomenon that landslides tend to happen where they have already occurred previously. That is, there could be factors that are not considered in the conventional model that explain the “where” of landslide occurrence better than the terrain attributes considered. For example, soil thickness or hydromechanical properties or climatic and environmental forcing factors that vary independently of topography. Thus, it is unclear how much the timing of previous landslides is relevant compared to merely the occurrence of past landslides. Perhaps this would be beyond the scope of this study, but it would be very interesting if the authors could somehow separate the spatial and temporal element to see how much of the model improvement is related to “landslides occur here” vs. “a landslide just occurred here” phenomena. This is interesting because it offers the possibility that historic landsliding (without a multi-temporal dataset) could be used as a variable to improve susceptibility modeling instead of trying to account for the difficult to measure subsurface variables. These points are worth mentioning in the discussion section to provide further context for the significance of the contribution and possible future directions.</p>	<p>Thank you for such a nice remark. Indeed this might be that the spatial part of path dependent model is not entirely related to the space-time effect of past landslides but could be partly because those places are unstable slopes where landslides keep occurring. The two landslide path dependency variables implemented in the conventional plus path dependent and purely path dependent landslide susceptibility models were derived simultaneously from Ripley's space-time k function in the line of joint spatial and temporal effect of landslide path dependency on future susceptibility, and are not separable with Ripley's function.</p> <p>In the revised manuscript, we have considered your point in the discussion as following:</p> <p>“The performance of this path dependency-only model thus highlights that proximity to previous landslides can adequately capture susceptible locations. It also suggests that the path dependent models' success in our experiments may be partly due to the fact that they capture static spatial effects that have not been resolved with our explanatory factors. It is attractive to imagine follow-up work that attempts to disentangle this static spatial effect that is unrelated to landslide history from dynamic spatial effects that are related to landslide history. The key to such disentangling should be that the former does not decay over time, whereas the latter does. More advanced statistical approaches that simultaneously estimate purely spatial and spatiotemporal effects may be needed.”</p>
<p>Specific Suggestions:</p> <p>L214. Here and elsewhere I suggest using the Oxford comma to appropriately distinguish between items in a list. It is used sometimes in the manuscript but not consistently.</p>	<p>We took care of this throughout the manuscript in the updated version.</p>
<p>Specific Suggestions:</p> <p>L225. Figure 6. What does the color red/green represent?</p>	<p>The colours represent the intensity of STC measure. We have added two sentences to the caption of figure 6 to make this clear as following:</p> <p>“The colours represent the intensity of STC measure. Red colour indicates high STC and green indicates low STC.”</p>
<p>Specific Suggestions:</p>	<p>Thank you for your observation. Indeed this is not immediately clear on the pie chart of only path</p>

<p>L270. Figure 7. In the Path dependent only case, there is clearly some red (0.8-1.0) on the map, but the pie chart indicates that 0% are in this class?</p>	<p>dependent map. The 0 % belongs to the probability class of 0-0.2 where is not computed in the only path dependent susceptibility map nor. The 0.32% belongs to the red colour in the map. We removed 0% and updated the map in the revised manuscript, and now the number is clear on the pie chart.</p>
<p>Specific Suggestions: L375. There are three models considered, so perhaps edit to: “In both improved models. . .”</p>	<p>Thank you for your suggestion, indeed that works better. We have edited that sentence to your suggested one.</p>
<p>Specific Suggestions: L381-387. It could be worth mentioning that precisely this phenomenon was observed at our site near Seattle (Mirus et al., 2017), namely for the same sequence of storm events a previous landslide remobilized multiple times whereas a neighboring hillslope with the same terrain attributes did not fail.</p>	<p>Indeed an example of observed dynamic susceptibility in your study area could be mentioned in that section of manuscript. We have added this point as following in the updated manuscript: “Such dynamics have been observed in a site near Seattle, Washington, where several new landslides occurred in a slope that had recently experienced landslide activity whereas a nearby hillslope with the same characteristics but without recently landslide activity did not experience new landsliding (Mirus et al., 2017).”</p>

1 **Dynamic path dependent landslide susceptibility modelling**

2 Jalal Samia ^{1,2}, Arnaud Temme ^{3,4}, Arnold Bregt ¹, Jakob Wallinga ², Fausto Guzzetti ⁵, Francesca Ardizzone ⁵

3 ¹ Laboratory of Geo-Information Science and Remote Sensing, Wageningen University & Research, 6708 PB
4 Wageningen, Droevendaalsesteeg 3, The Netherlands

5 ² Soil Geography and Landscape group, Wageningen University & Research, 6708 PB, Wageningen,
6 Droevendaalsesteeg 3, The Netherlands

7 ³ Department of Geography, Kansas State University, 920 N17th Street, Manhattan, KS, 66506, United States

8 ⁴ Institute of Arctic and Alpine Research, University of Colorado, Campus Box 450, Boulder, CO 803309-0450,
9 Colorado, United States

10 ⁵ Istituto di Ricerca per la Protezione Idrogeologica, Consiglio Nazionale delle Ricerche, via Madonna Alta 126,
11 06128 Perugia, Italy

12 **Correspondence:** Jalal Samia, jalal.samia@wur.nl, +31617699436, +31 (0)317 – 419000

13

14 **Abstract**

15 This contribution tests the added value of including landslide path dependency in statistically-based landslide
16 susceptibility modelling. A conventional pixel-based landslide susceptibility model was compared with a model
17 that includes landslide path dependency, and with a purely path dependent landslide susceptibility model. To
18 quantify path dependency among landslides, we used a Space-Time Clustering (STC) measure derived from
19 Ripley's space-time K function implemented on a point-based multi-temporal landslide inventory from the
20 Collazzone study area in central Italy. We found that the values of STC obey an exponential decay curve with
21 characteristic time scale of 17 years, and characteristic space scale of 60 meters. This exponential space-time decay
22 of the effect of a previous landslide on landslide susceptibility was used as the landslide path dependency
23 component of susceptibility models. We found that the performance of the conventional landslide susceptibility
24 model improved considerably when adding the effect of landslide path dependency. In fact, even the purely path
25 dependent landslide susceptibility model turned out to perform better than the conventional landslide susceptibility
26 model. The conventional plus path dependent and path dependent landslide susceptibility model and their resulted
27 maps are dynamic and change over time unlike conventional landslide susceptibility maps.

28

29 **1. Introduction**

30 Landslide susceptibility modelling calculates the likelihood of landslide occurrence in a certain location (Brabb,
31 1985). The resulting landslide susceptibility maps from landslide susceptibility models indicate where landslides
32 are likely to occur (Guzzetti et al., 2005). These maps are useful in land use planning and insurance, among others.
33 In this context, different methods and techniques have been used for landslide susceptibility modelling.

34 Reichenbach et al. (2018) classified these methods and techniques into five groups: (i) direct geomorphological
35 mapping, (ii) analysis of landslide inventories, (iii) heuristic or index-based approaches, (iv) physically or process-
36 based methods, and (v) statistically-based techniques.

37 Statistically-based landslide susceptibility techniques have been the preferred technique in the modelling of
38 landslide susceptibility (Reichenbach et al., 2018). In statistical landslide susceptibility modelling, empirical
39 quantitative relations are explored between the spatial distribution of landslides and a set of environmental factors
40 (e.g., slope and geology) (Van Westen et al., 2003; Guzzetti et al., 2005). The spatial distribution of historic
41 landslides, documented in landslides inventories, is therefore a crucial input for statistically-based landslide
42 susceptibility modelling (Guzzetti et al., 2012; Van Westen et al., 2008). Direct field mapping, visual interpretation
43 of aerial photographs, and other remote sensing images are the main sources for such mapping of landslide
44 inventories (Guzzetti et al., 2012). Landslides in such inventories are stored as points or polygons. Although
45 polygon-based landslide inventories (Ardizzone et al., 2018; Schlögel et al., 2011; Galli et al., 2008) are becoming
46 increasingly available, in many landslide prone regions only less-detailed point-based landslide inventories are
47 collected (Gorum et al., 2011; Sato et al., 2007; Keefer, 2000). Conditioning attributes used in landslide
48 susceptibility modelling are mainly derivatives of digital elevation models (DEMs) along with geological, soil,
49 and land use data (Günther et al., 2014; Neuhäuser et al., 2012; Reichenbach et al., 2018). While geology, land
50 use, and soil data are not always available in high detail, DEM-derivatives are easily computed and globally
51 available at a range of resolutions. Therefore, the minimum available dataset for landslide susceptibility modelling
52 includes a point-based landslide inventory and a set of DEM-derived conditioning attributes.

53 Traditionally, landslide susceptibility is considered time-invariant: susceptibility of a place to landslide occurrence
54 is constant over time, at least over decadal scales. Recently, we proposed the concept of time-variant landslide
55 susceptibility, where susceptibility changes over time due to the transient effect of previous landslides on future
56 landslide occurrence (Samia et al., 2017b, a). We referred to such a transient effect as “path dependency”, a term
57 adopted from complex system theory where it is used to describe the concept that the history of a system specifies
58 the future behaviour of a system through legacy effects (Phillips, 2006). In our study area in Umbria, central Italy
59 (Figure 1), we identified the existence of path dependency among landslides: earlier landslides locally increased
60 the susceptibility for future landslides for about two decades, during which the susceptibility decays exponentially
61 over time (Samia et al., 2017b). We first implemented the effect of this landslide path dependency in landslide
62 susceptibility modelling at the scale of slope units. Such units divide an area into hydrological units bounded by
63 drainage and divide lines (Carrara et al., 1991; Alvioli et al., 2016). We found that the impact of path dependency
64 on landslide susceptibility models at slope-unit scale was limited (Samia et al., 2018). This limited impact of
65 landslide path dependency on model predictions was probably due to the fact that landslide path dependency
66 affects landslide patterns at spatial scales smaller than slope units, and we hypothesized that differences between
67 models were likely to increase when including path dependency at smaller spatial scales.

68 The objective of this work is thus to consider the effect of landslide path dependency in landslide susceptibility
69 modelling at the resolution of 10×10 m pixels. We hypothesize that including landslide path dependency will
70 improve the performance of landslide susceptibility models. We also explore whether a purely path dependent
71 landslide susceptibility model, i.e. based solely on landslide inventory information, can provide a meaningful

72 landslide susceptibility map. We use the unique multi-temporal landslide inventory from the Collazzone study area
73 (Figure 1) (Guzzetti et al., 2006a; Ardizzone et al., 2007; Ardizzone et al., 2013).

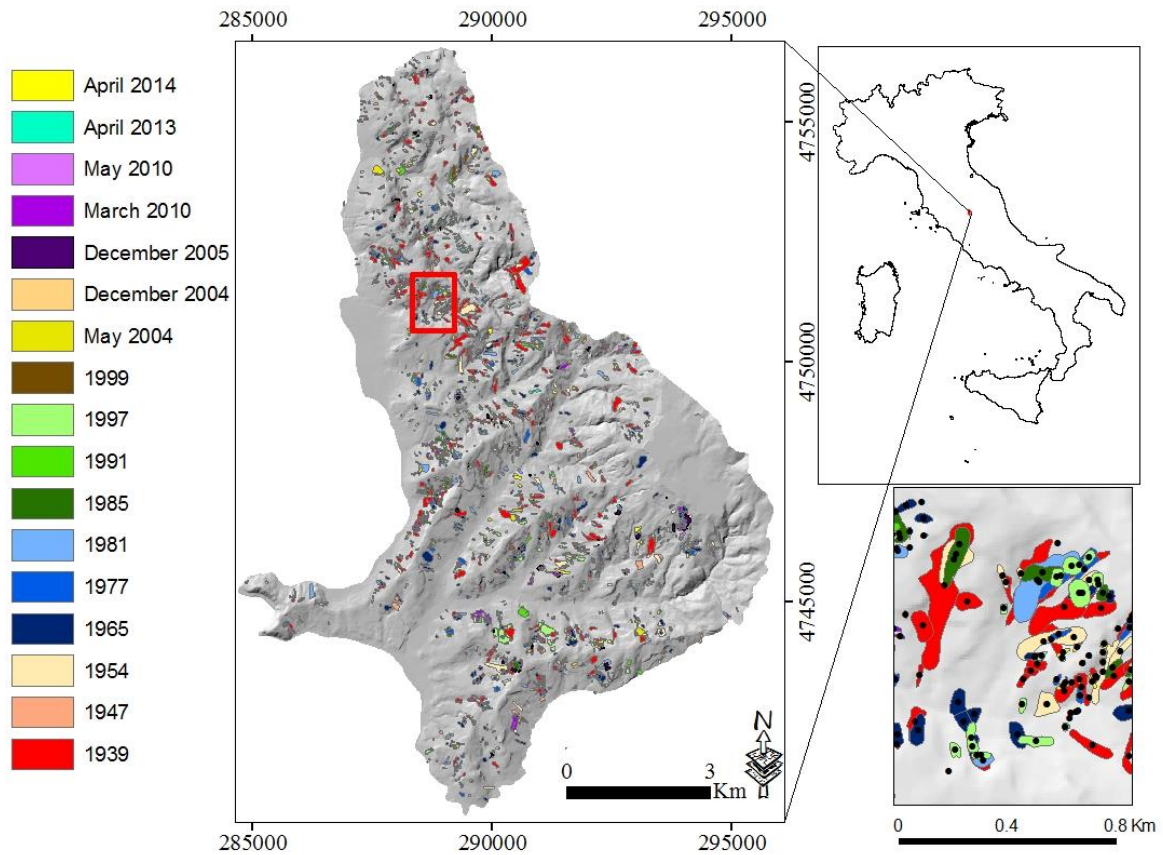
74 **2. Study area and data**

75 The Collazzone study area, Umbria, central Italy (Figure 1), extends for about 80 km² with terrain elevation
76 between 140 to 632 m and terrain slope derived from a 10 × 10 m DEM (Figure 2) between 0 to 64°. The DEM
77 was prepared by interpolating 5- and 10-m contour lines shown in 1:10,000 topographic maps (Guzzetti et al.,
78 2006b). A set of DEM-derivatives that has been widely used in landslide susceptibility modelling was computed
79 in SAGA GIS and ArcGIS. We expect that these DEM-derivatives capture topographical, geomorphological, and
80 hydrological properties of locations in our study area.

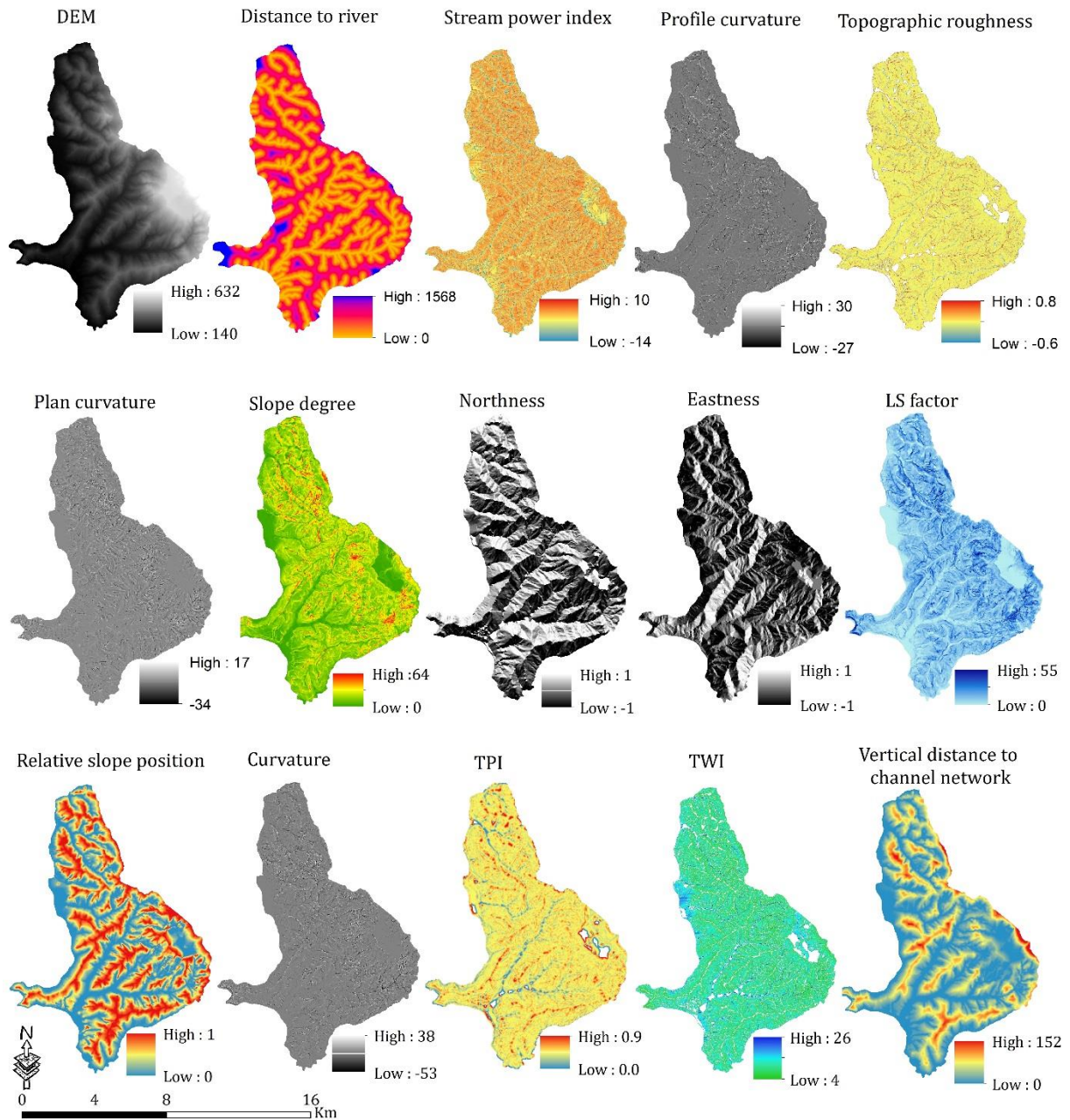
81 The DEM-derivatives (Figure 2) are slope angle, curvature, plan and profile curvature, aspect, northness and
82 eastness as cosine and sine transformations of aspect, topographic position index (TPI) representing different
83 geomorphological settings (Costanzo et al., 2012), stream power index (SPI) representing the erosive power of
84 streams (Moore et al., 1993), topographic wetness index (TWI) as an index for hydrological process in the slope
85 (Jebur et al., 2014). Additionally, for every pixel we computed the distance to the nearest river, the slope length
86 and steepness factor (LS factor) as an index for soil erosion on slope (Moore and Wilson, 1992), the vertical
87 distance to the slope's channel network, and relative slope position representing the relative position of slope in
88 cells between the valley bottom and ridgetop. Additionally, we calculated topographic roughness, which expresses
89 the difference in the values of elevation in the neighbouring cells in the DEM (Riley et al., 1999), and the standard
90 deviation of elevation and slope in a 3 × 3 pixel window. These 16 DEM-derivatives were used as independent
91 explanatory variables in logistic regression for modelling of landslide susceptibility (see section 3.2).

92 Landslides are abundant in this area, and range from recent shallow landslides to old deep-seated landslides
93 (Guzzetti et al., 2006a). Intense and prolonged rainfall and rapid snowmelt are the main triggers of landslides in
94 the area (Cardinali et al., 2000; Ardizzone et al., 2007). A unique multi-temporal landslide inventory with 3391
95 landslides has been mapped in 19 different time slices. The age of the landslides ranges from relict and very old
96 landslides with an uncertain date of occurrence to landslides that have occurred in 2014. Aerial photographs, direct
97 geomorphological field mapping, and satellite images were used for the preparation of the multi-temporal landslide
98 inventory (Ardizzone et al., 2013; Guzzetti et al., 2006a; Galli et al., 2008). Only time slices of the multi-temporal
99 inventory for which the relative date of occurrence is known (Figure 1), were used in this study because time
100 between landslides is a key element in the quantification of landslide path dependency (Samia et al., 2017a, b). In
101 addition, the first time slice, with the known date of 1939, was only used in the computation of the landslide path
102 dependency parameters, and not in landslide susceptibility modelling because of its unknown past. Ultimately, a
103 multi-temporal landslide inventory was used that contains distribution of landslides in 16 time slices dating from
104 1947 to 2014 (Figure 1). This multi-temporal landslide inventory was mostly prepared at the scale of 1:10,000
105 which is sufficient for conversion to a 10 × 10 m pixel-based landslide inventory. However, time slices from 1939
106 to 1997 were prepared from aerial photographs with scales ranging from 1:15,000 to 1:33,000, and this may
107 introduce some positional inaccuracy in landslides, in the order of one pixel. Given that the median size of landslide
108 in this period is 19 pixels, we believe that this is an acceptable level of inaccuracy.

109 More information about the Collazzone study area and the multi-temporal landslide inventory is given in (Galli et
110 al., 2008; Guzzetti et al., 2006a; Guzzetti et al., 2009; Ardizzone et al., 2007).



111
112 **Figure 1.** Multi-temporal landslide inventory dating from 1939 to 2014 (left map) (adapted from (Samia et al.,
113 2018)). Collazzone study area and Umbria region (right upper map). The coordinate system of maps is
114 EPSG:32633 (www.spatialreference.org). Landslide points were constructed by placing a point in the geometric
115 centre of each landslide polygon (map in the right lower corner). The red rectangle shows the extent of the map in
116 the lower right.



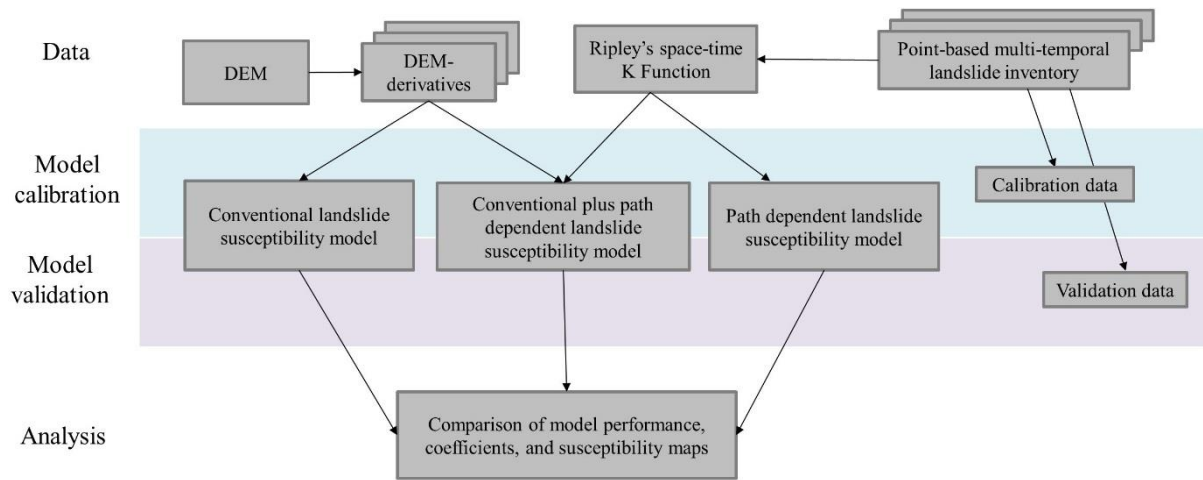
117

118 **Figure 2.** DEM (digital elevation model) and its derivatives used in conventional and conventional plus path
 119 dependent landslide susceptibility models. TPI means topographic position index, TWI means topographic wetness
 120 index, and LS factor stands for slope length and steepness factor.

121 **3. Methods**

122 We used logistic regression to construct three different landslide susceptibility models (Figure 3): (i) a
 123 conventional landslide susceptibility model using DEM-derivatives, (ii) a conventional plus path dependent
 124 landslide susceptibility model using 16 DEM-derivatives and two landslide path dependency variables (explained
 125 below), and (iii) a purely path dependent landslide susceptibility model using only the two landslide path
 126 dependency variables. We compared the performance of these models using Area Under Curve (AUC) values from
 127 the Receiver Operating Characteristic (ROC) (Mason and Graham, 2002), and selected the optimal model using

128 the Akaike Information Criterion (AIC) (Akaike, 1998), which penalizes the use of additional variables in a model.
 129 Ultimately, the coefficients of the variables selected by three landslide susceptibility models and the resulting
 130 landslide susceptibility maps were compared.



131 **Figure 3.** Flowchart of methods

132

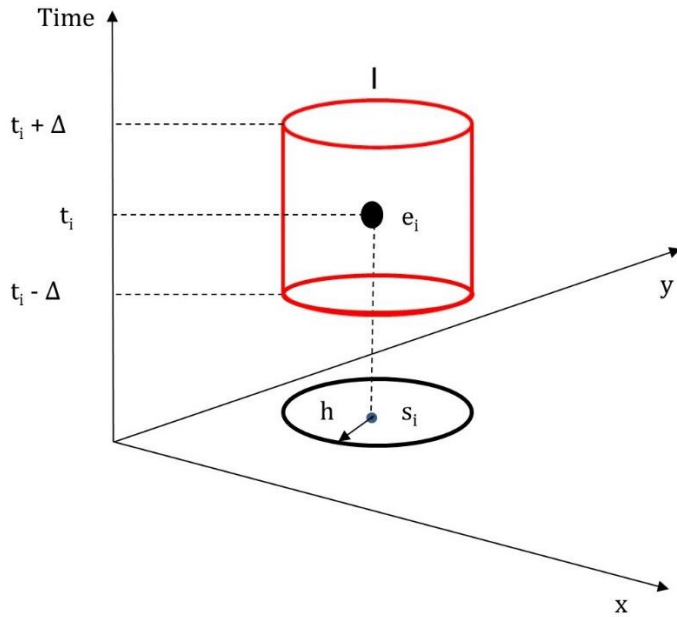
133 3.1 Quantifying landslide path dependency using Ripley's space-time K function

134 The spatial-temporal dynamics of landslide path dependency was recently quantified for the Collazzone study area
 135 (Samia et al., 2017a), and was implemented in landslide susceptibility modelling at the scale of slope units (Samia
 136 et al., 2018). Our previous quantification of landslide path dependency used simplified information about the
 137 spatial overlap among landslides in a polygon-based multi-temporal landslide inventory (Samia et al., 2017b). The
 138 novel aspect of the present paper is that now, at finer spatial resolution, we quantify landslide path dependency
 139 simultaneously in space and time. For this quantification, we use Ripley's K function (Ripley, 1976; Diggle et al.,
 140 1995). Ripley's K function has been used mainly in spatial point pattern analysis and reflects the degree of spatial
 141 clustering of events (e.g., landslides (Tonini et al., 2014), forest fire (Gavin et al., 2006), crimes (Levine, 2006),
 142 and disease outbreaks (Hinman et al., 2006)). The function determines whether events are clustered, dispersed,
 143 or randomly distributed. A modified Ripley's K function was also used to quantify the degree of clustering of point
 144 events in space and time (Lynch and Moorcroft, 2008; Ye et al., 2015). In the landslide path dependency context,
 145 we used Ripley's space-time K function to reflect the degree to which landslides occur near previous landslides,
 146 and how this changes with increasing distance to the previous landslide in space and time. The starting point to
 147 derive Ripley's K is a point-based multi-temporal landslide inventory consisting of points in the geometric centre
 148 of polygons of landslides (Figure 1).

149 Ripley's space-time K function tests whether the number of events that is observed in a space-time cylinder around
 150 an initial event is equal to what is expected given the average point density in space and time (Ripley, 1976, 1977;
 151 Diggle et al., 1995). The space-time cylinder $I_{(h, \Delta)}$ (Figure 4) is defined as:

$$152 I_{(h, \Delta)}(d_{ij}, t_{ij}) = \begin{cases} 1, & (d_{ij} \leq h \text{ and } (t_{ij} \leq \Delta)) \\ 0, & \text{otherwise} \end{cases} \quad (1)$$

153 where h shows the spatial distance increment, Δ shows the time increment, i and j are two landslide centre points,
 154 and d and t reflect the distance and time between the two landslide centre points, respectively.



155 **Figure 4.** Space-time cylinder neighbourhood (Smith, 2016) for a landslide event (e_i)

156 The expected Ripley's K function for one space-time cylinder of size h and Δ is defined as:

$$157 \quad K(h, \Delta) = \frac{1}{\lambda_{st}} \sum_{j \neq i} E[I_{(h, \Delta)}(d_{ij}, t_{ij})] \quad (2)$$

158 where E is the expected number of landslides in the cylinder, and λ_{st} reflects the average space-time intensity of
 159 the landslides i.e., the expected number of landslides per unit of space-time volume, which is calculated as:

$$160 \quad \lambda_{st} = \frac{n}{a(R) \times (t_{max} - t_{min})} \quad (3)$$

161 where n is the number of landslides in the entire inventory, t is time, and $a(R)$ reflects the size of the area. Therefore,
 162 the expected Ripley's space-time K function for the space-time cylinders around each landslide point is defined
 163 as:

$$164 \quad K(h, \Delta) = \frac{1}{n \cdot \lambda_{st}} \sum_{i=1}^n \sum_{j \neq i} E[I_{(h, \Delta)}(d_{ij}, t_{ij})] \quad (4)$$

165 Similarly, the observed Ripley's space-time K function is calculated from the landslide inventory as:

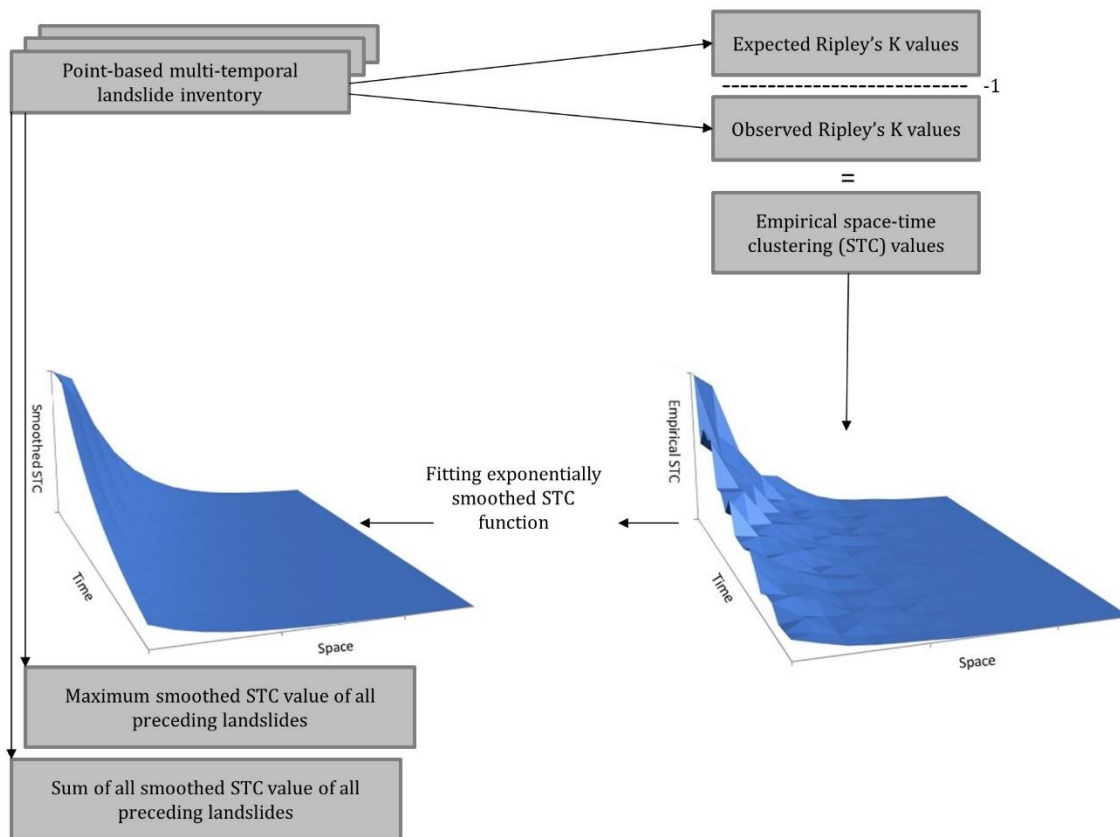
$$166 \quad \hat{K}(h, \Delta) = \frac{1}{n \cdot \lambda_{st}} \sum_{i=1}^n \sum_{j \neq i} I_{(h, \Delta)}(d_{ij}, t_{ij}). \quad (5)$$

167 Finally, we defined the space-time clustering (STC) measure, which reflects how much more likely it is that a
 168 landslide will occur given a time and space distance from a previous landslide, as following:

$$169 \quad \text{Empirical } STC(h, \Delta) = \frac{\hat{K}(h, \Delta)}{K(h, \Delta)} - 1 \quad (6)$$

170 STC values > 0 indicate clustering and values < 0 indicate dispersion. We calculated STC (h, Δ) for a wide range
 171 of h and Δ : values of h ranged from 0 to 500 meter in 30 steps, and values of Δ ranged from 0 to 38 years in 30
 172 steps. This yielded 900 empirical values of STC (h, Δ). We then fitted an exponential decay function of h and Δ to
 173 the empirical STC values. This exponential decay function was used to calculate STC values for each pixel
 174 depending on when and where a landslide last occurred closely to that pixel.

175 Based on this, we calculated two landslide path dependency variables. The first variable reflects the maximum
 176 value of all STC values for all previous landslides near a pixel. This variable results in high values when one
 177 particular previous nearby landslide is expected to have a large impact on the susceptibility of landsliding. The
 178 second variable is the sum of all STC values of all previous landslides near a pixel. This variable results in high
 179 values when all previous nearby landslides are expected to have a large impact on the susceptibility of landsliding.
 180 This approach mirrors what we did in our slope unit-based susceptibility model (Samia et al., 2018) in the sense
 181 that the variables separate the impact of the most impactful previous nearby landslide from the impacts of all
 182 previous nearby landslides.



183 **Figure 5.** Procedure to compute the two landslide path dependency variables using Ripley's space-time K function.

184 **3.2 Logistic regression**

185 Logistic regression is considered a reference model in statistically-based landslide susceptibility modelling
 186 (Reichenbach et al., 2018). Relations between presence and absence of landslides as a binary target variable are
 187 explained by a set of independent variables such as slope steepness and slope position in logistic regression. In

188 this paper, DEM-derivatives (section 2 and Figure 2) as well as the two landslide path dependency variables
189 computed using the Ripley's space-time K function (see section 3.1) were used as independent variables. Landslide
190 presence or absence was the binary target variable.

191 **3.3 Training and testing**

192 When using a multi-temporal landslide inventory in landslide susceptibility modelling, the selection of time slices
193 for the training and testing is crucial. In Rossi et al. (2010) and Samia et al. (2018), a sequential splitting sampling
194 strategy was used in such a way that landslides in older time slices were used to train the model and landslides in
195 newer time slices were used to test the model. However, such a sequential sampling strategy does not provide an
196 equal range of landslide histories between training and testing datasets, and this could bias the role of time in path
197 dependent landslide susceptibility modelling. To avoid such a timing inequality, Samia et al. (2018) also
198 introduced a non-sequential sampling strategy in which the span of timing segregation among time slices in the
199 training and the testing datasets is comparable. In this study, we used this sampling strategy to split the multi-
200 temporal landslide inventory into training and testing datasets. To achieve this, landslides in the time slices of
201 1947, 1954, 1981, 1985, 1999, May 2004, March, and May 2010 were used for training, and landslides in the time
202 slices of 1965, 1977, 1991, 1997, December 2004 and 2005 and April 2013 and 2014 were used for testing (Figure
203 1). It is important to note that the time slice in 1939 was used only for quantification of landsliding history of the
204 other time slices, and not for training or testing. Thus, the 1st time slice in the training dataset is 1947 (Figure 1).

205 The number of pixels with landslides was smaller than the number of pixels without landslides in both training
206 and testing datasets. Therefore, we randomly selected 5,000 pixels with landslides and 5,000 pixels without
207 landslides to create equal datasets for training and testing. This random selection of pixels was repeated 10 times
208 both in the training and testing datasets. After preparation of the 10 training datasets, logistic regression was
209 applied to the 10 training datasets with entry probability of 0.05 and removal probability of 0.06 for independent
210 variables to diminish the chance of overfitting in the model. We only allowed inter-variable correlations less than
211 0.8 to avoid multicollinearity. Model performance was assessed using AUC and AIC values. The AUC values for
212 testing were assessed using 10 training models and 10 independent testing datasets. The models with highest
213 performance in terms of AUC values, were used to map susceptibility to landslides. Finally, we compared landslide
214 susceptibility maps resulting from conventional, conventional plus path dependent, and purely path dependent
215 susceptibility.

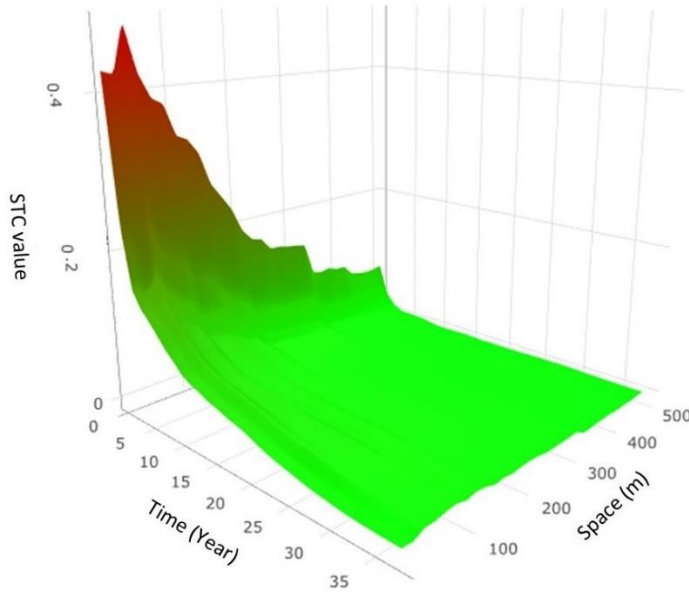
216 **4. Results**

217 **4.1 Spatial-temporal dynamic of landslide path dependency**

218 Ripley's space-time K function confirmed the existence of landslide path dependency at small spatial and small
219 temporal distances from a previous landslide (Figure 6). The STC measure (Eq 6) is high in the space-time vicinity
220 of an earlier landslide, and it then decreases rapidly. Apparently, landslide susceptibility is relatively high
221 immediately after occurrence of an earlier, nearby landslide.

222

223



225 **Figure 6.** Space-time dynamic of landslide path dependency. The colours represent the intensity of STC measure.
 226 Red colour indicates high STC and green indicates low STC.

227 The exponential decay function that was fitted to the empirical STC values is:

228 $Smoothed\ STC(t, d) = 0.44 * e^{(-t/16.7)} * e^{(-d/58.8)} \quad (7)$

229 This function shows that the STC measure decays exponentially over a characteristic time scale of 16.7 years and
 230 characteristic spatial scale of 58.8 meters. The residual standard error of the exponential function is 0.01, in units
 231 of STC (-), which compares favourably with the actual values that range up to 0.44.

232 **4.2 Model performance**

233 We compared performance of the conventional, conventional plus path dependent, and purely path dependent
 234 landslide susceptibility models, using AUC (greater is better) and AIC (lower is better) values as measure of
 235 performance. The best performing landslide susceptibility model was the conventional plus path dependent model,
 236 both when expressed as AUC values and as AIC values (Table 1). The purely path dependent landslide
 237 susceptibility model, constructed with only the two landslide path dependency variables, performed better than the
 238 conventional landslide susceptibility model with its 16 DEM-derived variables.

239 **Table 1.** Performance of the three landslide susceptibility models

AUC and AIC values	Conventional susceptibility model	Conventional plus path dependent susceptibility model	Path dependent susceptibility model
AUC training	0.704 ± 0.006	0.764 ± 0.003	0.721 ± 0.004
AIC training	12,678 ± 82	11,711 ± 53	12,469 ± 62
AUC testing	0.682 ± 0.007	0.732 ± 0.004	0.698 ± 0.004

241 For conventional susceptibility models, 6 DEM-derivatives were selected in all 10 models (Table 2). Adding two
 242 landslide path dependency variables into DEM-derivatives variables affected the inclusion and exclusion of DEM-
 243 derivative variables only slightly. For example, the variables TPI and distance to river were selected 4 and 7 times
 244 respectively in the conventional susceptibility models whereas after adding the two landslide path dependency
 245 variables, these variables were selected 5 and 4 times respectively. The variable eastness which was selected twice
 246 in the conventional susceptibility models, was never selected in the conventional plus path dependent susceptibility
 247 models.

248 **Table 2.** Selection of independent variables in conventional, conventional plus path dependent, and purely path
 249 dependent landslide susceptibility modelling. Variables selected 6 or more times are shown. The numbers between
 250 parentheses indicate how often variables were selected.

Three landslide susceptibility models	Number of variables selection in 10 times repetition	Average number of variables selected in the three susceptibility models
Conventional (16 DEM-derivatives)	Elevation (10), standard deviation of slope (10), LS factor (10), standard deviation of elevation (10), stream power index (10), aspect (10), distance to river (7), vertical distance to channel network (6), relative slope position (6)	8.7
Conventional plus path dependent (16 DEM-derivatives plus two landslide path dependency variables)	Elevation (10), standard deviation of slope (10), LS factor (10), standard deviation of elevation (10), stream power index (10), aspect (10), max smoothed STC value (10), sum of all smoothed STC value (10)	10.4
Path dependent (two landslide path dependency variables)	max smoothed STC value (10), sum of all smoothed STC value (10)	2

251

252 In all the training and the testing datasets, the contingency tables (Table 3) showed that conventional landslide
 253 susceptibility models differed substantially from the conventional plus path dependent and path dependent
 254 landslide susceptibility models. In particular, the percentage of false positives (the percentage of pixels without
 255 landslides predicted with landslides) for the conventional susceptibility models is higher than for the two other
 256 susceptibility models. However, there are also fewer true negatives (the percentage of pixels without landslides
 257 predicted without landslides) in the conventional than in the conventional plus path dependent and path dependent
 258 susceptibility models. The variation in the differences is larger in the training datasets than the testing datasets,
 259 suggesting that all fitted models are robust.

260

261
 262
 263
 264

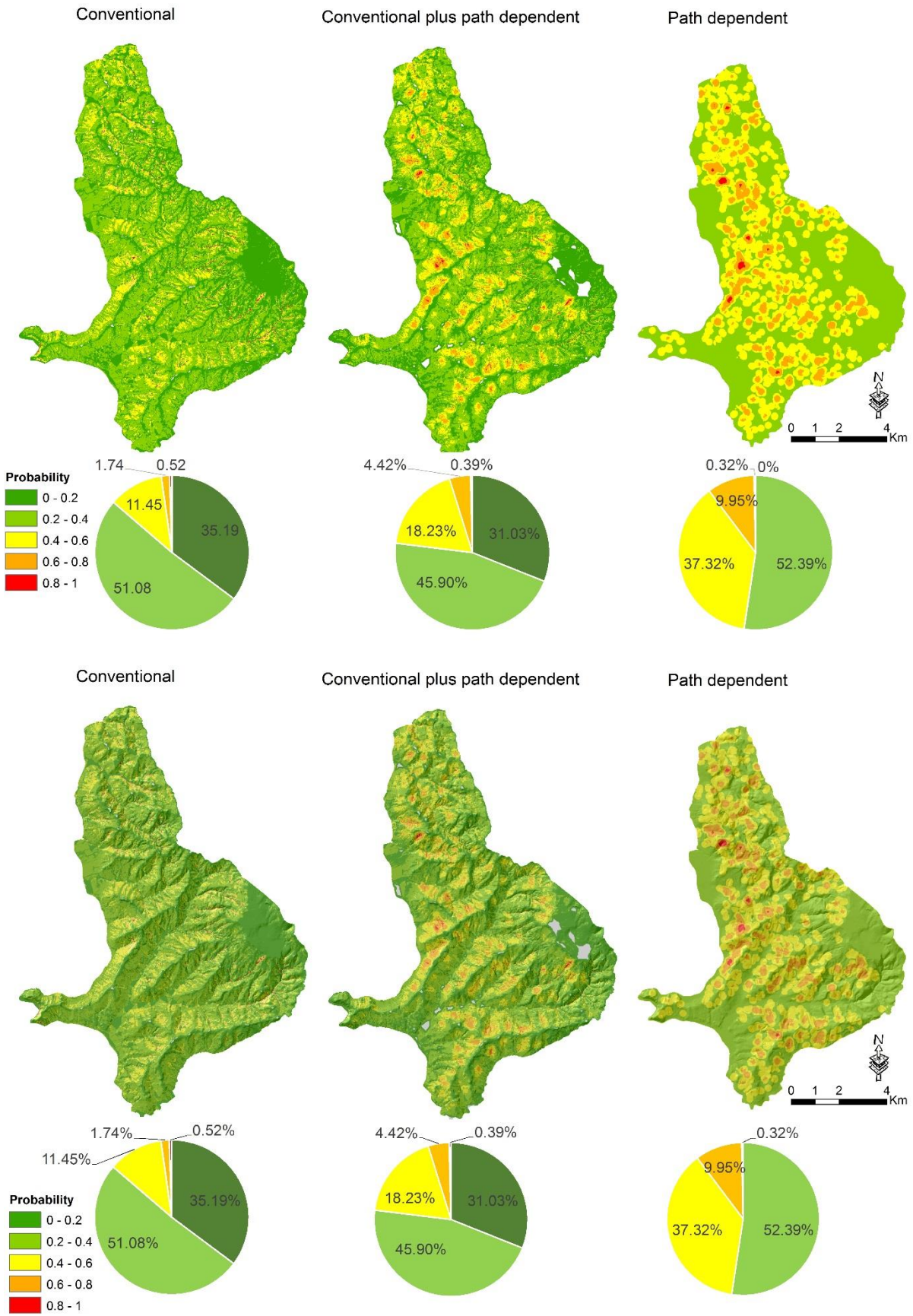
Table 3. Contingency tables computed with cut off value of 0.5 for the three models.

		Conventional landslide susceptibility		Conventional plus path dependent landslide susceptibility		Path dependent landslide susceptibility	
		Observed landslides		Observed landslides		Observed landslides	
		yes	no	yes	no	yes	no
Predicted landslides (training)	yes	35 ± 0.33	19 ± 0.60	34 ± 0.42	14 ± 0.23	31 ± 0.8	13 ± 0.32
	no	15 ± 0.33	31 ± 0.60	16 ± 0.42	36 ± 0.23	19 ± 0.8	37 ± 0.32
Predicted landslides (testing)	yes	33 ± 0.50	19 ± 0.21	29 ± 0.35	13 ± 0.43	23 ± 0.24	12 ± 0.41
	no	17 ± 0.50	31 ± 0.21	21 ± 0.35	37 ± 0.43	27 ± 0.24	38 ± 0.41

265
 266
 267
 268
 269
 270
 271
 272
 273
 274
 275

3.3 Conventional, conventional plus path dependent and purely path dependent landslide susceptibility maps

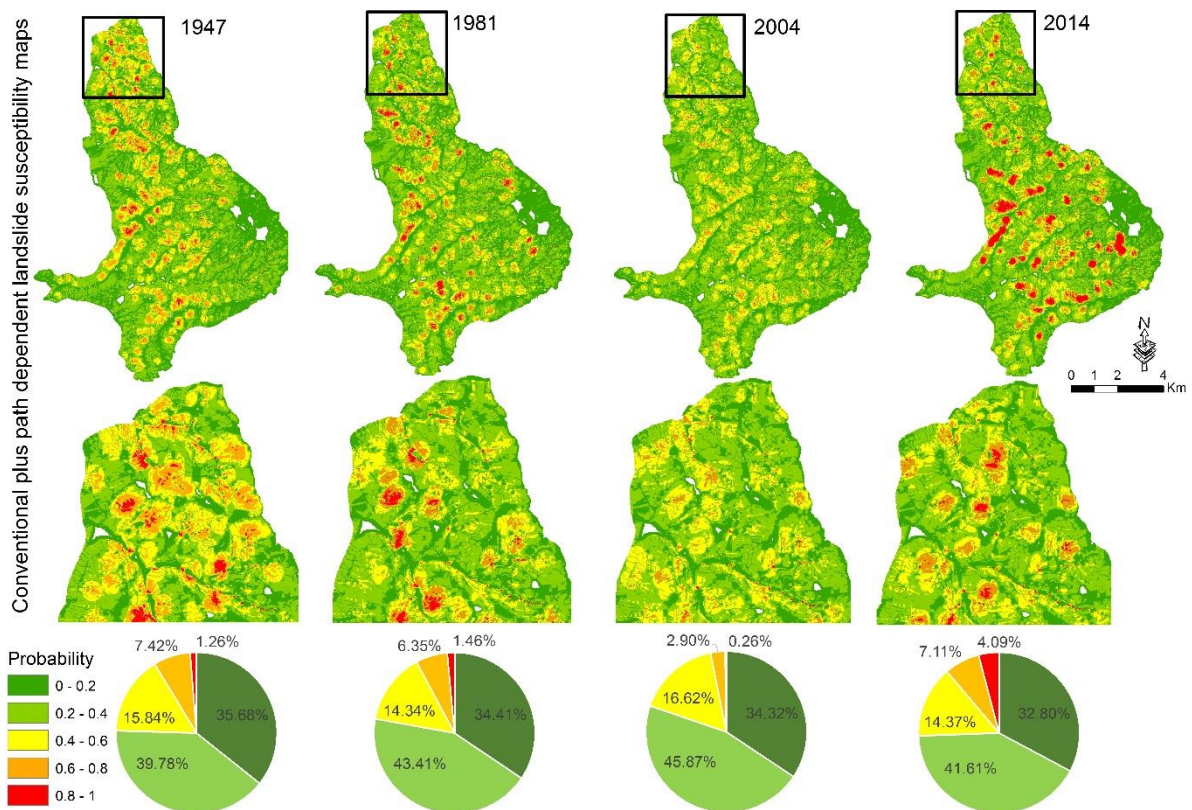
The landslide susceptibility maps derived from the three models illustrate different patterns of landslide susceptibility (Figure 7). For the models that include path dependency, the presented maps give the average values of all simulated time slices. Differences between the maps correspond with the considerable differences in the performance of their landslide susceptibility models in terms of AUC and AIC values (Table 1). The path dependent landslide susceptibility map is visually different from both other landslide susceptibility maps, with the pattern dominated by regions of high susceptibility around locations where landslides previously occurred.



276 **Figure 7.** Conventional landslide susceptibility map in the left, the conventional plus path dependent landslide
 277 susceptibility map (averaged out over 16 time slices) in the middle, and path dependent landslide susceptibility

278 map (averaged out over 16 time slices) in the right. The pie charts show the percentage of pixels in each map in
 279 different probability levels of landslide occurrence.

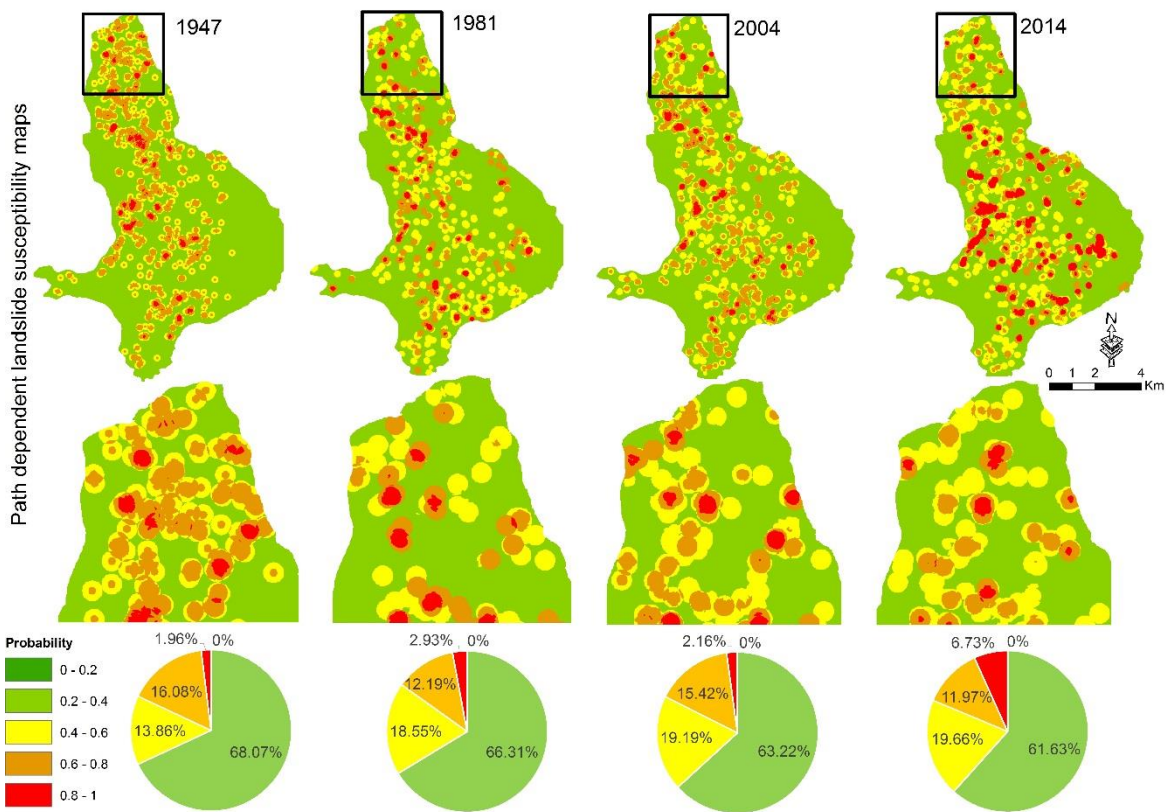
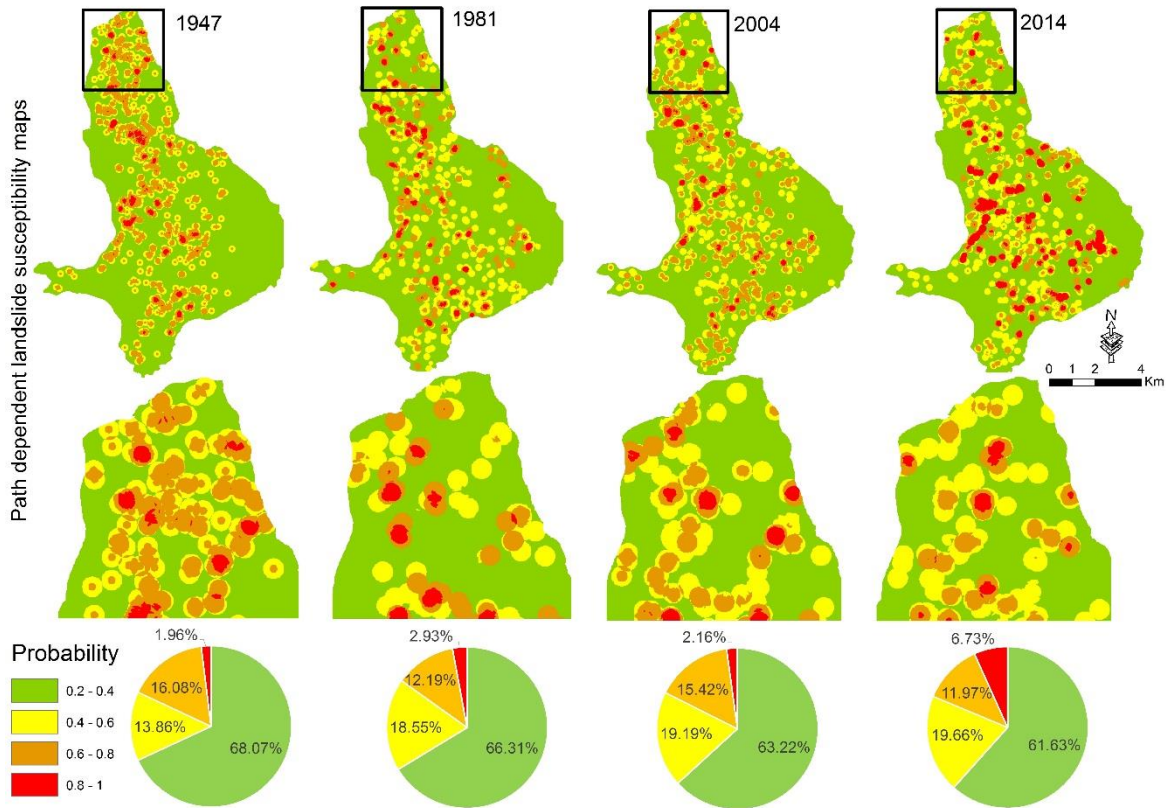
280 The 16 conventional plus path dependent landslide susceptibility maps are dynamic and change over time (Figure
 281 8). These changes reflect the exponential decay with increasing time since previous nearby landslides (Figure 6)
 282 and the sudden increase of susceptibility in areas close to recent landslides. The gradual decrease in susceptibility
 283 levels is clearest when comparing the 1981 and 2004 susceptibility maps, whereas the sudden increase is clearest
 284 when comparing the 2004 and 2014 maps. The 2014 susceptibility map has higher susceptibility levels because of
 285 the impact of recent landslides in the year 2013.



286
 287 **Figure 8.** Examples of four dynamic conventional plus path dependent landslide susceptibility maps in the years
 288 of 1947, 1981, 2004 and 2014. Zoomed maps show the places where there are large changes in susceptibility over
 289 time.

290 Similar dynamics are visible when comparing landslide susceptibility maps constructed with the purely path
 291 dependent model for different years (Figure 9). These maps show only the pure influence of earlier landslides on
 292 susceptibility to future landslides (Figure 6). Again, the susceptibility of landslides decreases where distance from
 293 earlier landslides in space and time increases, but jumps back up when more recent landslides become part of the
 294 landslide history. The pure influence of each individual landslide on the susceptibility to the future landslide is
 295 strong when a landslide is fresh which is reflected in the high percentage of susceptibility levels of 0.6-0.8 and
 296 0.8-1.0 in 1947 and 2014. When time passes since the previous landslide has occurred, the susceptibility decreases

297 with an exponential decay response which is reflected in the low percentage of susceptibility levels of 0.6-0.8 and
 298 0.8-1.0 in 1981 and 2004.



299 **Figure 9.** Examples of four dynamic path dependent landslide susceptibility maps in the years of 1947, 1981, 2004
300 and 2014. Zoomed maps show the places where there are large changes in susceptibility over time.

301 **5. Discussion**

302 In this section, we focus first on the quantification of landslide path dependency in the pixel-based multi-temporal
303 landslide inventory, and then discuss its role in susceptibility models. We also discuss the susceptibility model
304 performance for all three model types. At the end, the exportability of landslide path dependency parameters and
305 the implication of dynamic time-variant path dependent landslide susceptibility in landslide hazard is discussed.

306 **5.1 Quantification of landslide path dependency**

307 The quantification of landslide path dependency using Ripley's space-time K function (Ripley, 1976; Diggle et
308 al., 1995) indicates, in our study area, an exponential decay response in the STC values (Figure 6). This means
309 that there is a positive influence of earlier nearby landslides on susceptibility that decays exponentially in time and
310 space with a characteristic time scale of about 17 years, and a characteristic space scale of about 60 meters. This
311 is in accordance with our previously quantified landslide path dependency using follow-up landslide fraction in
312 which the decay period of landslide path dependency was found to be about two decades (Samia et al., 2017b).
313 Landslide clustering manifests in the form of spatial association among landslides where follow-up landslides
314 occur immediately after and close to a previous landslide (Samia et al., 2017a). Samia et al. (2017b) discussed the
315 possible mechanism in the formation of clusters of landslides in which the size of the initial landslide and changes
316 in hydrology of slope destabilized by a landslide could facilitate the occurrence of follow-up landslides and hence
317 clusters of landslides.

318 STC values and their exponential decay to some extent depend on the method that we have chosen to determine
319 the centre point of landslides when converting polygons of landslides to points of landslides. Our approach was to
320 take the geometric centre, but other options exist (Haines, 1994) and their impact should be explored. Also, in the
321 computation of STC values with Ripley's space-time K function, distance between landslides was calculated using
322 the Pythagorean theorem without distinguishing between distances in the x and y direction. Also we did not include
323 differences in the elevation of centre points in our distance calculations. For future work, it could be interesting to
324 define one dimension as the distance along the slope in the downslope direction and another dimension as the
325 distance in the slope parallel direction, and keeping these two spatial dimensions separate in addition to the
326 temporal dimension.

327 **5.2 Effect of landslide path dependency on performance of landslide susceptibility models**

328 Our results demonstrated that including landslide path dependency effect in a pixel-based landslide susceptibility
329 model constructed by DEM-derivatives improves model performance substantially. This is in line with high AUC
330 and low AIC values for the conventional plus path dependent landslide susceptibility model (Table 1). This
331 confirms our main hypothesis that adding the effect of landslide path dependency boosts the performance of
332 landslide susceptibility models, and is in accordance with our previous expectations regarding stronger effect of
333 landslide path dependency in a pixel-based landslide susceptibility model than in a slope unit-based landslide
334 susceptibility model (Samia et al., 2018). Landslide path dependency is a local effect (apparently with
335 characteristic space scale of about 60 meters) in which an earlier landslide increases the likelihood of follow-up

336 landslide occurrence. Such a local effect is obviously more visible at pixel resolution of 10 m rather than at slope
337 unit resolution (with a median size of 51486 m² in our study area).

338 Strikingly, the purely path dependent landslide susceptibility model constructed with only the two landslide path
339 dependency variables performs better than the conventional landslide susceptibility model made by DEM-
340 derivative variables (Table 1). This is potentially interesting since this implies that the landslide inventory itself
341 can be used to map susceptibility to landslide without using DEM-derivatives which have been conventionally
342 used in landslide susceptibility modelling (Varnes, 1984; Guzzetti et al., 2005). The performance of this path
343 dependency-only model thus highlights that proximity to previous landslides can adequately capture susceptible
344 locations. It also suggests that the path dependent models' success in our experiments may be partly due to the fact
345 that they capture static spatial effects that have not been resolved with our explanatory factors. It is attractive to
346 imagine follow-up work that attempts to disentangle this static spatial effect that is unrelated to landslide history
347 from dynamic spatial effects that are related to landslide history. The key to such disentangling should be that the
348 former does not decay over time, whereas the latter does. More advanced statistical approaches that simultaneously
349 estimate purely spatial and spatiotemporal effects may be needed.

350

351 Another important aspect of considering landslide path dependency effect in landslide susceptibility modelling is
352 providing dynamic landslide susceptibility maps. Landslide susceptibility maps are usually classified into five
353 levels of probability to landslide occurrence ranging from 0 to 1. In the conventional landslide susceptibility map
354 (Figure 7, right map), the five probability levels of susceptibility by definition remain constant over time since the
355 DEM-derivatives in the model are constant (although DEM-derivatives also change when a landslide occurs, but
356 DEMs are not updated frequently enough to reflect this). In reality, susceptibility maps created with this time-
357 insensitive method are used in planning only for an amount of time roughly equal to the temporal length of the
358 original landslide inventory.

359 However, adding landslide path dependency in landslide susceptibility models, provides dynamic landslide
360 susceptibility maps (Figures 8 and 9) in which the levels of susceptibility change over time, reflecting the
361 exponential decay response of landslide path dependency (Figure 6). The changes are in the places where
362 landslides have already occurred, mainly in probability levels of susceptibility ranging from 0.6 to 1.0. This
363 suggests that the part of area located in the high probability level of susceptibility could switch to the low
364 probability level of susceptibility (0 to 0.6) after a decade. This is exemplified between 1947 and 1954 landslide
365 susceptibility maps, in which about 9 km² of study area drops more than 0.1 in their probability of landslide
366 occurrence. After adding the two path dependency variables in the conventional landslide susceptibility modelled
367 with DEM-derivatives, it turns out that the coefficients of all DEM-derivative variables become lower (e.g., LS
368 factor becomes less important).

369 **5.3 Can landslide path dependency parameters be transported to other areas?**

370 In landslide prone areas where landslides are documented and mapped in the form of polygon-based multi-
371 temporal inventories, the landslide path dependency can be quantified based on geographical overlap among
372 landslides, and hence used in landslide susceptibility modelling (Samia et al., 2017b; Samia et al., 2018). However,

373 polygon-based multi-temporal landslide inventories are rare to the best of our knowledge, and hence in many areas
374 geographical overlap among landslides cannot be computed. In this paper, we proposed using Ripley's space-time
375 K function to compute landslide path dependency where point-based multi-temporal landslide inventories are used.
376 Using such inventories, our STC measure (Eq. 6) can be used to quantify path dependency among landslides.

377 It is attractive to think that the STC measure (Eq. 6) and its parameters (Eq. 7) can be directly exported to landslide
378 prone areas with substantial geological and topographical similarities. However, to gain confidence in this
379 approach, multi-temporal landslide inventories from such places (e.g., (Schlögel et al., 2011)) need to be
380 interrogated to find out whether path dependency occurs, whether it occurs over similar space and time scales, and
381 whether it adds value to susceptibility modelling. This would also allow us to start exploring what determines the
382 characteristic space and time scales.

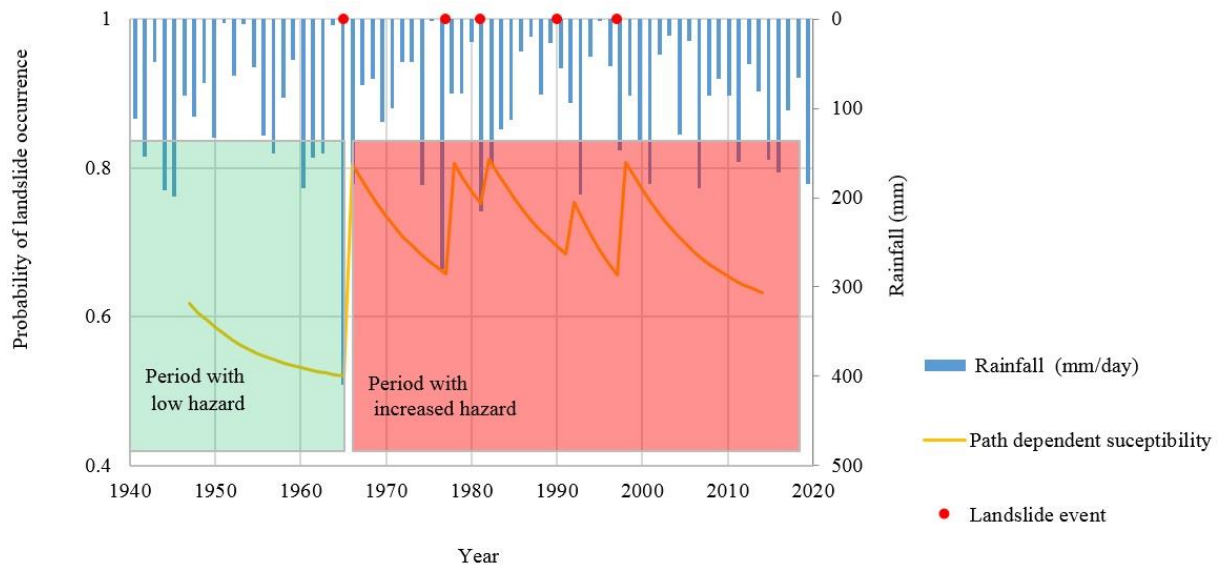
383 **5.4 Implications of path dependent landslide susceptibility in landslide hazard assessment**

384 We have already modified the definition of conventional landslide susceptibility modelling (Varnes, 1984;
385 Guzzetti et al., 2005) using spatial temporal dynamics of landslide path dependency (Samia et al., 2017a, b) as
386 following:

$$387 \text{Landslide susceptibility}_{s,t} = f(\text{conditioning attributes}_s, \text{landslide path dependency}_{s,t}) \quad (8)$$

388 In this study, both conventional plus path dependent and path dependent landslide susceptibility models turned out
389 to perform better than a conventional landslide susceptibility model (Table 1). In both improved models,
390 availability of a space-time component – reflecting the exponential decay of landslide path dependency – indicates
391 that landslide susceptibility is dynamic. This challenges the way landslide hazard is assessed as landslide
392 susceptibility is an important element of landslide hazard.

393 In landslide hazard assessment, landslide susceptibility as a proxy of 'where landslides occur' is combined with
394 the temporal probability of landslide triggers (mainly rainfall) to determine 'when landslides occur' (Guzzetti et
395 al., 2006a). In this context, a dynamic landslide susceptibility (Eq. 8) needs to be considered in combination with
396 the temporal information of landslide triggers in the assessment of landslide hazard. When substantial landsliding
397 happens during a rainfall event, susceptibility in and around such landslides can be raised for a few decades in
398 which moderate rainfall events may already cause substantial landsliding, which raises susceptibility levels again.
399 (Figure 10). Such dynamics have been observed in a site near Seattle, Washington, where several new landslides
400 occurred in a slope that had recently experienced landslide activity whereas a nearby hillslope with the same
401 characteristics but without recently landslide activity did not experience new landsliding (Mirus et al., 2017).
402 If no substantial triggering event happens over the characteristic time scale of roughly 17 years, the increased
403 susceptibility will be substantially reduced, and a later rainfall event may have less influence on landsliding; the
404 probability of experiencing a follow-up landslide will have decreased.



405 **Figure 10.** Hypothetical example of the implication of dynamic path dependent landslide susceptibility model in
 406 landslide hazard assessment. When susceptibility is low, the hazard is also low (providing the other components
 407 of landslide hazard e.g., size remain unchanged) and large rainfall events are needed to trigger new landslides.
 408 Then, when susceptibility is raised by such landslides, the hazard is also high and small rainfall events may trigger
 409 new landslides.

410 6. Conclusion

411 In the Collazzone study area, in Central Italy, quantification of landslide path dependency reveals an exponential
 412 decay response in landslide susceptibility as a function of space and time distance to earlier nearby landslides. For
 413 our study area, the characteristic time scale of this effect is about 17 years and the characteristic space scale is
 414 about 60 meters. Adding such an exponential decay response of landslide path dependency in conventional pixel-
 415 based landslide susceptibility modelled by DEM-derivative improves the performance of model substantially.
 416 Taking into account landslide path dependency effects in landslide susceptibility results in dynamic landslide
 417 susceptibility models where susceptibility changes over time. We stress that landslide susceptibility modelling
 418 should take the effect of landslide path dependency into account since it provides an estimation of temporal
 419 validation of different probability levels of landslide occurrence in landslide susceptibility map. The obtained
 420 landslide path dependency parameters can possibly be used for dynamic landslide susceptibility modelling in
 421 landslide prone areas with environmental and data similarities. We proposed a conceptual model that considers
 422 the impact of dynamic path dependent landslide susceptibility on landslide hazard.

423 Acknowledgement

424 This research is part of J Samia PhD project at Wageningen University and Research, funded by Ministry of
 425 Science, Research and Technology of Iran, Laboratory of Geo-Information Science and Remote Sensing and Soil
 426 Geography & Landscape group of Wageningen University, and supported by the Geography Department of Kansas
 427 State University in USA.

428

- 430 Akaike, H.: Information theory and an extension of the maximum likelihood principle, in: Selected Papers of
431 Hirotugu Akaike, Springer, 199-213, 1998.
- 432 Alvioli, M., Marchesini, I., Reichenbach, P., Rossi, M., Ardizzone, F., Fiorucci, F., and Guzzetti, F.: Automatic
433 delineation of geomorphological slope units with r.slopeunits v1.0 and their optimization for landslide
434 susceptibility modeling, *Geosci. Model Dev.*, 9, 3975-3991, 10.5194/gmd-9-3975-2016, 2016.
- 435 Ardizzone, F., Cardinali, M., Galli, M., Guzzetti, F., and Reichenbach, P.: Identification and mapping of recent
436 rainfall-induced landslides using elevation data collected by airborne Lidar, *Natural Hazards and Earth System
437 Science*, 7, 637-650, 2007.
- 438 Ardizzone, F., Fiorucci, F., Santangelo, M., Cardinali, M., Mondini, A. C., Rossi, M., Reichenbach, P., and
439 Guzzetti, F.: Very-high resolution stereoscopic satellite images for landslide mapping, in: *Landslide science and
440 practice*, Springer, 95-101, 2013.
- 441 Ardizzone, F., Fiorucci, F., Mondini, A. C., and Guzzetti, F.: TXT-tool 1.039-1.1: Very-High Resolution Stereo
442 Satellite Images for Landslide Mapping, in: *Landslide Dynamics: ISDR-ICL Landslide Interactive Teaching Tools
443 : Volume 1: Fundamentals, Mapping and Monitoring*, edited by: Sassa, K., Guzzetti, F., Yamagishi, H., Arbanas,
444 Ž., Casagli, N., McSaveney, M., and Dang, K., Springer International Publishing, Cham, 83-94, 2018.
- 445 Brabb, E. E.: Innovative approaches to landslide hazard and risk mapping, *International Landslide Symposium
446 Proceedings*, Toronto, Canada, 1985, 17-22,
- 447 Cardinali, M., Ardizzone, F., Galli, M., Guzzetti, F., and Reichenbach, P.: Landslides triggered by rapid snow
448 melting: the December 1996–January 1997 event in Central Italy, *Proceedings 1st Plinius Conference on
449 Mediterranean Storms*, 2000, 439-448,
- 450 Carrara, A., Cardinali, M., Detti, R., Guzzetti, F., Pasqui, V., and Reichenbach, P.: GIS techniques and statistical
451 models in evaluating landslide hazard, *Earth surface processes and landforms*, 16, 427-445, 1991.
- 452 Costanzo, D., Rotigliano, E., Irigaray Fernández, C., Jiménez-Perálvarez, J. D., and Chacón Montero, J.: Factors
453 selection in landslide susceptibility modelling on large scale following the gis matrix method: application to the
454 river Beiro basin (Spain), 2012.
- 455 Diggle, P. J., Chetwynd, A. G., Häggkvist, R., and Morris, S. E.: Second-order analysis of space-time clustering,
456 *Statistical methods in medical research*, 4, 124-136, 1995.
- 457 Galli, M., Ardizzone, F., Cardinali, M., Guzzetti, F., and Reichenbach, P.: Comparing landslide inventory maps,
458 *Geomorphology*, 94, 268-289, 2008.
- 459 Gavin, D. G., Hu, F. S., Lertzman, K., and Corbett, P.: WEAK CLIMATIC CONTROL OF STAND-SCALE FIRE
460 HISTORY DURING THE LATE HOLOCENE, *Ecology*, 87, 1722-1732, 2006.
- 461 Gorum, T., Fan, X., van Westen, C. J., Huang, R. Q., Xu, Q., Tang, C., and Wang, G.: Distribution pattern of
462 earthquake-induced landslides triggered by the 12 May 2008 Wenchuan earthquake, *Geomorphology*, 133,
463 152-167, <https://doi.org/10.1016/j.geomorph.2010.12.030>, 2011.
- 464 Günther, A., Van Den Eeckhaut, M., Malet, J.-P., Reichenbach, P., and Hervás, J.: Climate-physiographically
465 differentiated Pan-European landslide susceptibility assessment using spatial multi-criteria evaluation and
466 transnational landslide information, *Geomorphology*, 224, 69-85,
467 <https://doi.org/10.1016/j.geomorph.2014.07.011>, 2014.
- 468 Guzzetti, F., Reichenbach, P., Cardinali, M., Galli, M., and Ardizzone, F.: Probabilistic landslide hazard
469 assessment at the basin scale, *Geomorphology*, 72, 272-299, 2005.
- 470 Guzzetti, F., Galli, M., Reichenbach, P., Ardizzone, F., and Cardinali, M.: Landslide hazard assessment in the
471 Collazzone area, Umbria, Central Italy, *Natural Hazards and Earth System Science*, 6, 115-131, 2006a.
- 472 Guzzetti, F., Reichenbach, P., Ardizzone, F., Cardinali, M., and Galli, M.: Estimating the quality of landslide
473 susceptibility models, *Geomorphology*, 81, 166-184, <https://doi.org/10.1016/j.geomorph.2006.04.007>, 2006b.
- 474 Guzzetti, F., Ardizzone, F., Cardinali, M., Rossi, M., and Valigi, D.: Landslide volumes and landslide mobilization
475 rates in Umbria, central Italy, *Earth and Planetary Science Letters*, 279, 222-229,
476 <https://doi.org/10.1016/j.epsl.2009.01.005>, 2009.
- 477 Guzzetti, F., Mondini, A. C., Cardinali, M., Fiorucci, F., Santangelo, M., and Chang, K.-T.: Landslide inventory
478 maps: New tools for an old problem, *Earth-Science Reviews*, 112, 42-66, 2012.
- 479 Haines, E.: Point in polygon strategies, *Graphics gems IV*, 994, 24-26, 1994.
- 480 Hinman, S. E., Blackburn, J. K., and Curtis, A.: Spatial and temporal structure of typhoid outbreaks in
481 Washington, DC, 1906–1909: evaluating local clustering with the G_i^* statistic, *International Journal of Health
482 Geographics*, 5, 13, 2006.
- 483 Jebur, M. N., Pradhan, B., and Tehrany, M. S.: Optimization of landslide conditioning factors using very high-
484 resolution airborne laser scanning (LiDAR) data at catchment scale, *Remote Sensing of Environment*, 152, 150-
485 165, 2014.
- 486 Keefer, D. K.: Statistical analysis of an earthquake-induced landslide distribution — the 1989 Loma Prieta,
487 California event, *Engineering Geology*, 58, 231-249, [https://doi.org/10.1016/S0013-7952\(00\)00037-5](https://doi.org/10.1016/S0013-7952(00)00037-5), 2000.
- 488 Levine, N.: Crime mapping and the Crimestat program, *Geographical analysis*, 38, 41-56, 2006.
- 489 Lynch, H. J., and Moorcroft, P. R.: A spatiotemporal Ripley's K-function to analyze interactions between spruce
490 budworm and fire in British Columbia, Canada, *Canadian Journal of Forest Research*, 38, 3112-3119, 2008.
- 491 Mason, S. J., and Graham, N. E.: Areas beneath the relative operating characteristics (ROC) and relative
492 operating levels (ROL) curves: Statistical significance and interpretation, *Quarterly Journal of the Royal
493 Meteorological Society*, 128, 2145-2166, 2002.
- 494 Mirus, B. B., Smith, J. B., and Baum, R. L.: Hydrologic Impacts of Landslide Disturbances: Implications for
495 Remobilization and Hazard Persistence, *Water Resources Research*, 53, 8250-8265, 10.1002/2017wr020842,
496 2017.
- 497 Moore, I. D., and Wilson, J. P.: Length-slope factors for the Revised Universal Soil Loss Equation: Simplified
498 method of estimation, *Journal of soil and water conservation*, 47, 423-428, 1992.

499 Moore, I. D., Gessler, P., Nielsen, G., and Peterson, G.: Soil attribute prediction using terrain analysis, *Soil*
500 *Science Society of America Journal*, 57, 443-452, 1993.

501 Neuhäuser, B., Damm, B., and Terhorst, B.: GIS-based assessment of landslide susceptibility on the base of the
502 weights-of-evidence model, *Landslides*, 9, 511-528, 2012.

503 Phillips, J.: Evolutionary geomorphology: thresholds and nonlinearity in landform response to environmental
504 change, 2006.

505 Reichenbach, P., Rossi, M., Malamud, B. D., Mihir, M., and Guzzetti, F.: A review of statistically-based landslide
506 susceptibility models, *Earth-Science Reviews*, 180, 60-91, <https://doi.org/10.1016/j.earscirev.2018.03.001>,
507 2018.

508 Riley, S. J., DeGloria, S., and Elliot, R.: Index that quantifies topographic heterogeneity, *intermountain Journal*
509 *of sciences*, 5, 23-27, 1999.

510 Ripley, B. D.: The second-order analysis of stationary point processes, *Journal of applied probability*, 13, 255-
511 266, 1976.

512 Ripley, B. D.: Modelling spatial patterns, *Journal of the Royal Statistical Society. Series B (Methodological)*,
513 172-212, 1977.

514 Rossi, M., Guzzetti, F., Reichenbach, P., Mondini, A. C., and Peruccacci, S.: Optimal landslide susceptibility
515 zonation based on multiple forecasts, *Geomorphology*, 114, 129-142,
516 <https://doi.org/10.1016/j.geomorph.2009.06.020>, 2010.

517 Samia, J., Temme, A., Bregt, A., Wallinga, J., Guzzetti, F., Ardizzone, F., and Rossi, M.: Do landslides follow
518 landslides? Insights in path dependency from a multi-temporal landslide inventory, *Landslides*, 14, 547-558,
519 10.1007/s10346-016-0739-x, 2017a.

520 Samia, J., Temme, A., Bregt, A., Wallinga, J., Guzzetti, F., Ardizzone, F., and Rossi, M.: Characterization and
521 quantification of path dependency in landslide susceptibility, *Geomorphology*, 292, 16-24,
522 <https://doi.org/10.1016/j.geomorph.2017.04.039>, 2017b.

523 Samia, J., Temme, A., Bregt, A. K., Wallinga, J., Stuijver, J., Guzzetti, F., Ardizzone, F., and Rossi, M.:
524 Implementing landslide path dependency in landslide susceptibility modelling, *Landslides*, 1-16, 2018.

525 Sato, H. P., Hasegawa, H., Fujiwara, S., Tobita, M., Koarai, M., Une, H., and Iwahashi, J.: Interpretation of
526 landslide distribution triggered by the 2005 Northern Pakistan earthquake using SPOT 5 imagery, *Landslides*, 4,
527 113-122, 10.1007/s10346-006-0069-5, 2007.

528 Schlögel, R., Torgoev, I., De Marneffe, C., and Havenith, H. B.: Evidence of a changing size–frequency
529 distribution of landslides in the Kyrgyz Tien Shan, Central Asia, *Earth Surface Processes and Landforms*, 36,
530 1658-1669, 2011.

531 Smith, T.: Notebook on spatial data analysis, Lecture Note, 2016.

532 Tonini, M., Pedrazzini, A., Penna, I., and Jaboyedoff, M.: Spatial pattern of landslides in Swiss Rhone Valley,
533 *Natural Hazards*, 73, 97-110, 2014.

534 Van Westen, C., Rengers, N., and Soeters, R.: Use of geomorphological information in indirect landslide
535 susceptibility assessment, *Natural hazards*, 30, 399-419, 2003.

536 Van Westen, C. J., Castellanos, E., and Kuriakose, S. L.: Spatial data for landslide susceptibility, hazard, and
537 vulnerability assessment: an overview, *Engineering geology*, 102, 112-131, 2008.

538 Varnes, D. J.: *Landslide hazard zonation: a review of principles and practice*, 1984.

539 Ye, X., Xu, X., Lee, J., Zhu, X., and Wu, L.: Space–time interaction of residential burglaries in Wuhan, China,
540 *Applied Geography*, 60, 210-216, <https://doi.org/10.1016/j.apgeog.2014.11.022>, 2015.

541